Mineralogical Magazine (2021), **85**, 262–277
doi:10.1180/mgm.2021.11

CAMBRIDGE UNIVERSITY PRESS

Article

Evolution of fumarolic anhydrous copper sulfate minerals during successive hydration/dehydration

Oleg I. Siidra[1]*, Artem S. Borisov[1], Dmitri O. Charkin[2], Wulf Depmeier[3] and Natalia V. Platonova[4]

[1]Department of Crystallography, St. Petersburg State University, University Embankment 7/9, 199034 St. Petersburg, Russia; [2]Chemistry Department, Moscow State University, Leninskie Gory 1-3, Moscow 199992 Russia; [3]Institut für Geowissenschaften der Universität Kiel, Olshausenstr. 40, D-24098 Kiel, Germany; and [4]X-ray Diffraction Resource Center, St. Petersburg State University, University Embankment 7/9, 199034 St. Petersburg, Russia

Abstract

Hydration processes of primary anhydrous minerals as well as dehydration of the hydrated phases are relevant not only for answering geochemical and petrological questions, but are also interesting in the context of the theory of the 'Evolution of minerals'. Our study of the evolution of anhydrous exhalative sulfates in hydration and dehydration processes has demonstrated the complexity of the processes for a number of minerals from the active high-temperature fumaroles of Tolbachik volcano (chalcocyanite $Cu(SO_4)$, dolerophanite $Cu_2O(SO_4)$, alumoklyuchevskite $K_3Cu_3AlO_2(SO_4)_4$ and itelmenite $Na_2CuMg_2(SO_4)_4$). Hydration and dehydration experiments were carried out for all four minerals using powder X-ray diffraction. A typical structural characteristic of several anhydrous copper sulfate minerals of fumarolic origin is the presence of oxygen-centred OCu_4 tetrahedra. These are absent in the structures of all known hydrated minerals or synthetic compounds of the class under consideration. Hydration of minerals initially containing O^{2-} anions as part of oxocomplexes, proceeds with sequential formation of a large series of hydroxysalts. On the contrary, hydration of itelmenite with its relatively complex 'initial' structure, but without additional oxygen atoms that are strong Lewis bases, results in formation of simpler hydrates. The lower the temperature and the larger the excess of water, the stronger the tendency of the cations to adopt higher hydration numbers thus outcompeting the sulfate anions as ligands. Ultimately, the water molecules completely expel the bridging sulfate anions from the metal coordination sphere yielding relatively simple fully hydrated structures.

Keywords: evolution of minerals, sulfates, reversible hydration/dehydration, fumarolic minerals, X-ray diffraction

(Received 19 November 2020; accepted 28 January 2021; Accepted Manuscript published online: 2 February 2021; Associate Editor: Ferdinando Bosi)

Introduction

Hydration processes of primary anhydrous minerals as well as dehydration of the hydrated phases are relevant not only for answering geochemical and petrological questions, but are also interesting in the context of the theory of the 'Evolution of minerals' (Hazen *et al.*, 2008). One important piece of this theory refers to the observation that new mineral species formed by hydration are usually more complex than the pristine ones, and often more than one secondary species are formed from a given primary mineral. There are many more important aspects of hydration/oxidation processes, e.g. their role in the formation of economic mineral deposits or their possible ecological threat, as these processes are often the first steps of destructive weathering that can lead to release of toxic elements into the environment with all kinds of subsequent detrimental effects.

In the past few decades, hydration and dehydration processes of sulfate minerals, especially those containing iron, have been studied (Sklute *et al.*, 2018; Xu *et al.*, 2009). Much systematic work has been devoted to the study of hydration and dehydration processes in the magnesium–sulfate–water system, in view of understanding the palaeo-atmospheric conditions on Mars (e.g. Vaniman *et al.*, 2004; Chipera and Vaniman, 2007; Altheide *et al.*, 2009; Grevel and Majzlan, 2009). Note that all of the cited publications – and others not cited here for lack of space – concern primarily simple systems such as $Fe(SO_4)$–$H_2(SO_4)$–H_2O or $Mg(SO_4)$–$H_2(SO_4)$–H_2O. Systems containing other cations, e.g. other transition metals instead of Fe, or additional main group cations such as Na or K, or anions like halides, have received less attention to date.

Anhydrous high-temperature sulfate minerals with transition metals such as iron, copper, zinc and vanadium are quite exotic mineral species, and occur almost exclusively in fumaroles of active volcanoes – in a few cases they also form by natural underground coal fires (e.g. Pautov *et al.*, 2020). These minerals often become unstable under changing temperature conditions and are particularly unstable when they are exposed to humid atmosphere or to precipitation. When this happens they may hydrate rapidly and undergo various chemical and physical transformations, including repeated dissolution–crystallisation cycles. Re-heating by exhausting hot gases from the fumarole may lead to dehydration with either recovery of the pristine minerals, or crystallisation of new species. The chemical compositions as well as the structural architectures of many fumarolic minerals are unique and have no analogues among synthetic compounds,

*Author for correspondence: Oleg I. Siidra, Email: o.siidra@spbu.ru
Cite this article: Siidra O.I., Borisov A.S., Charkin D.O., Depmeier W. and Platonova N.V. (2021) Evolution of fumarolic anhydrous copper sulfate minerals during successive hydration/dehydration. *Mineralogical Magazine* **85**, 262–277. https://doi.org/10.1180/mgm.2021.11

which makes them also interesting for inorganic crystal chemistry and materials science. Equally of interest is the possible occurrence of metastable transient phases upon hydration or dehydration, which are often inaccessible via traditional synthetic routes.

Fumaroles on active volcanoes can be subdivided into two groups: (1) fumaroles with oxidising conditions and (2) fumaroles with reducing mineral-formation environments. The latter are much more common and have been well-studied in terms of mineralogy; common primary mineral species are native elements, sulfides and sulfosalts. Overall, the mineral inventory is relatively poor and uniform. In stark contrast to the latter, oxidising fumaroles are much less common on Earth and they differ significantly in the number and variety of mineral species. Some of the best-studied fumaroles with oxidising conditions are located at the Vesuvius volcano where they show remarkable copper oxide mineralisation (Balassone *et al.*, 2019). The Vesuvius fumaroles have been known since antiquity. In the middle of the 20th Century, oxidising fumaroles of the Izalco volcano in Salvador were investigated and revealed rich anhydrous copper–vanadium mineralisation (Hughes and Stoiber, 1985). Half a century ago, in 1975–1976, one of the most famous eruptions of the 20th Century rocked the Tolbachik volcano located on the Kamchatka Peninsula, Russian Federation. This became known as the Great Fissure Tolbachik Eruption (Fedotov and Markhinin, 1983). Several scoria cones were formed and the associated fumaroles turned out to be real bonanzas providing amazingly rich and diverse mineral associations, which have become a veritable playground for the study of the mineralogy and crystal chemistry of volcanic exhalations (Vergasova and Filatov, 2012, 2016; Pekov *et al.*, 2018 a,b). In 2012, another important eruption occurred on the Tolbachik volcano – the Fissure Tolbachik Eruption. The copper mineralisation in the fumaroles of the Second Scoria Cone of the Great Fissure Tolbachik Eruption was so rich that at the end of the 1970s these fumaroles were valued as a very rich, though small, copper deposit and possible mining was considered. Fortunately, the remoteness and inaccessibility of this deposit made its possible exploitation uneconomic. The fumaroles became world-renowned, not so much as a reservoir of copper, but rather for the large number of different endemic mineral species, as well as for the total mineral diversity, which makes it second to none on our planet, at least to this date. Note that the areas holding productive fumaroles are rather small: the fumarole field on the Second Scoria Cone for example extends over just a few hundred square metres. Nevertheless, more than 110 new mineral species have been described from the fumaroles of Great Fissure Tolbachik Eruption and the Fissure Tolbachik Eruption to date. We also contributed to this list by the discovery and study of a number of new anhydrous sulfate mineral species from the fumaroles of both localities (Siidra *et al.*, 2014a, 2017, 2018a,b,c, 2019b,c, 2020a,b; Nazarchuk *et al.*, 2018, 2020). It is very likely that the list of new minerals discovered in the fumaroles of the Tolbachik volcano is far from complete. Post-eruptive processes are still ongoing and the formation of new mineral species is being observed. The temperature in the fumaroles is by no means constant but changes over time, either rising or falling. Some of the fumaroles that were active decades ago, are now extinct. As a result of alteration by hydration processes, the formation of unique associations of secondary hydrated sulfate minerals has been observed (e.g. Siidra *et al.*, 2014b,c). However, the transformation of primary fumarolic minerals under the influence of atmospheric moisture has been poorly studied to date. The temperature regime in the upper fumarole zones is subject to seasonal fluctuations due to the large amount of atmospheric precipitations. The first systematic studies of these processes were carried out by our group on euchlorine $KNaCu_3O(SO_4)_3$ (Siidra *et al.*, 2019a), which demonstrated an unexpected complexity of such processes, both in the number of phases formed and in the transformations of multiphase aggregates as a function of changing temperatures. The current paper expands these studies to cover a larger set of fumarolic minerals.

The Yadovitaya (Russian for 'Poisonous') fumarole (55°49′59″N, 160°19′59″E) is located in the fumarole field on the summit of the Second Scoria Cone of the Northern Breakthrough of the Great Fissure Tolbachik Eruption. The field is located ~18 km SSW from the active shield volcano Ploskiy (flat) Tolbachik (Fedotov and Markhinin, 1983). The Yadovitaya fumarole was one of the first fumaroles described after the Great Fissure Tolbachik Eruption (Vergasova and Filatov, 2016). The intensity of the gas streams in this fumarole varied greatly in the first years after the eruption (Menyailov *et al.*, 1980a) and Yadovitaya fumarole is still very active to date. The diversity in the number of endemic copper sulfate mineral species with various additional cations and anions in the Yadovitaya fumarole is impressive. Figure 1a shows a photograph of the freshly cleared fumarole wall to a depth of 2.5 metres as of September 2019. The Cu–SO_4 zone enriched in various anhydrous copper sulfates ranges from 35 cm to 65–70 cm below the top of the fumarole; marked by red lines on Fig. 1a. All the mineral samples (Fig. 1b,d,e) used for hydration experiments described below were collected from this zone. The temperature of exhaust gases registered on the level of the Cu–SO_4 zone was ~300°C. All the samples recovered were packed and isolated immediately after collection in order to protect them from contact with the external atmosphere. It is clearly evident that chalcocyanite, dolerophanite and alumoklyuchevskite were deposited directly as sublimates from volcanic gas emissions, however the origin of itelmenite, which contains a significant amount of Mg, is presumed to be the product of a reaction between volcanic gases and the basaltic scoria. This is corroborated by the fact that possible relevant Mg compounds have very low volatility at 300°C, hence direct sublimation of this mineral is deemed improbable. On the top of the fumarole, on the outcrop, there is a zone (~10 cm) with variable fluoride mineralisation. Between the fluoride zone and the Cu–SO_4 zone, a 15 to 25 cm thick intermediate zone composed of altered and hydrated copper sulfate minerals is easily discerned by its colouration (Fig. 1).

Hydration experiments and high-temperature powder X-ray crystallography

Experimental

Chalcocyanite, dolerophanite, alumoklyuchevskite and itelmenite are water soluble and sensitive to air humidity. The crystals of all minerals start to alter, with initial formation of hydrated mineral films, after only one day of exposure (e.g. chalcocyanite) to open air with 81% relative humidity and 23°C. Systematic hydration experiments were carried out to monitor the occurring transformations by powder X-ray diffraction (PXRD).

For all the minerals used for further research, qualitative electron microprobe analysis (Hitachi S-3400N scanning electron microscope equipped with an Oxford Instruments X-Max 20 Energy Dispersive Spectrometer) revealed no elements other than reported in the respective publications: chalcocyanite (Siidra *et al.*, 2018a), alumoklyuchevskite (Gorskaya *et al.*, 1995,

https://doi.org/10.1180/mgm.2021.11 Published online by Cambridge University Press

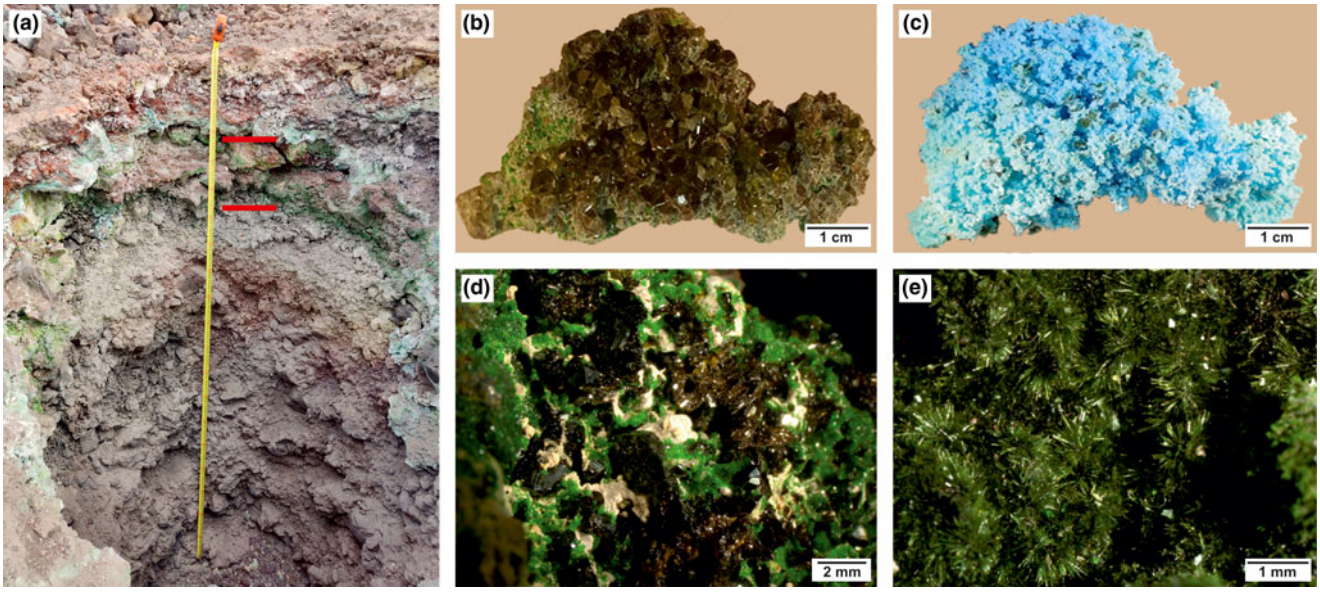

Fig. 1. General view of the wall of the Yadovitaya fumarole. The Cu–SO_4 rich zone is delimited by red lines (a). The maximum thickness of the Cu–SO_4 zone is 35 cm. Well crystallised chalcocyanite sample excavated from this zone (b) and the same sample, almost completely transformed into chalcanthite, exposed to humid air for one week (c). Dark brown crystals of dolerophanite with green euchlorine (d) and clusters of needle-like crystals of alumoklyuchevskite (e) from the Cu–SO_4 zone used in this work.

Siidra *et al.*, 2017) and itelmenite (Nazarchuk *et al.*, 2018). There is a published semi-quantitative chemical analysis of dolerophanite from the fumaroles of Vesuvius (Kahler, 1962). The dolerophanite sample used in this study contained 1.8 wt.% ZnO. An admixture of zinc is rather common for the copper sulfate minerals studied here. This is not surprising as the gas condensates of the Great Fissure Tolbachik Eruption were highly enriched in Zn (Menyailov *et al.*, 1980a,b). Apart from the slight Zn-for-Cu substitution in dolerophanite, the ratio of the elements in the minerals agrees well with the formulas, *viz.* chalcocyanite $Cu(SO_4)$, dolerophanite $Cu_2O(SO_4)$, alumoklyuchevskite $K_3Cu_3AlO_2(SO_4)_4$ and itelmenite $Na_2CuMg_2(SO_4)_4$.

The experiments for all four minerals were carried out using the same technique: 1 g of each mineral was hand-picked under an optical microscope and ground in an agate mortar. Prior to that the purity of each sample was checked using PXRD, and in the case of observed impurities a new sample was selected. The pure powdered sample was loaded on a Si plate for further X-ray measurements. In turn, the holder with the Si plate was placed inside a common desiccator (3 litre volume) and 250 ml of distilled water was poured into the bottom of the desiccator. The humidity in the desiccator during the experiments was monitored by a humidity- and temperature-meter CEM DT-625. The estimated standard deviation (e.s.d.) for humidity values is 0.5%. Each set of experiments was repeated twice. In total six subsequent stages of hydration were carried out for each mineral and the results are listed in Tables 1, 3 and 5. The transformation of each powder sample into the respective single phase or mixture of hydrated sulfates is accompanied by colour changes (Figs 2–5).

A Rigaku Ultima X-ray diffractometer (Cu*K*α radiation) was used to give PXRD data in air after each stage. The duration of each X-ray measurement was ~15 min. The evolution of the powder diffraction patterns in moist environments is shown in Figs 2–5. Full powder diffraction patterns were collected at different intervals and analysed via Rietveld refinement using the *TOPAS* program (Bruker, 2014). Using the known structural data for each of the intermediate phases (minerals) listed in Tables 1–6 it was possible to refine the phase fraction of each of the intermediate phases and thus to determine the composition of the mixtures. Note, all mineral-like phases that appear during hydration/dehydration are in quotes.

The thermal behaviour of the mixtures of the different hydrated sulfates was studied subsequently in air by means of a Rigaku Ultima X-ray diffractometer (Co*K*α radiation (dolerophanite, alumoklyuchevskite and itelmenite experiments) or Cu*K*α radiation (chalcocyanite experiment only) and a high-temperature camera Rigaku HTA 1600. The sample was loaded on a Pt–Rh plate. Temperature steps were 25°C in the range 25–400°C. The evolution of the PXRD patterns during heating is shown in Figs 2–5. The phases identified at different steps are listed in Tables 2,4 and 6.

Results

Chalcocyanite $Cu(SO_4)$

Hydration

In a moist atmosphere chalcocyanite transforms rapidly into 'chalcanthite' $Cu(SO_4)\cdot 5H_2O$ (Bacon and Titterton, 1975). The single-phase composition remains intact until the last stage of the hydration (Fig. 2).

Dehydration

The first stage of heating (Fig. 2) at 25°C and 50°C is also characterised by chalcanthite. However, note that the first minor peaks of 'bonattite' $Cu(SO_4)\cdot 3H_2O$ (Zahrobsky and Baur, 1968) start to appear at 50°C. At 75°C, the sample completely consists of 'bonattite' $Cu(SO_4)\cdot 3H_2O$. The third stage covers the relatively large temperature range 100°C–200°C and is characterised also by a single-phase corresponding to 'poitevinite' $Cu(SO_4)\cdot H_2O$ (Ting *et al.*, 2009). At 225°C a transitional stage with coexisting 'poitevinite' and anhydrous $CuSO_4$ (chalcocyanite) is observed. Starting

https://doi.org/10.1180/mgm.2021.11 Published online by Cambridge University Press

Table 1. Evolution of primary dolerophanite into mixtures of hydrated sulfates during the hydration experiments at 23°C, different duration and different relative humidity.

Stage 1 Initial sample	Stage 2 30 min, humidity 85%	Stage 3 30 min, humidity 86%	Stage 4 60 min, humidity 88%	Stage 5 120 min, humidity 90%	Stage 6 30 min, humidity 91%	Stage 7 14 hours, humidity 94%
dolerophanite 100	**'dolerophanite' 47** **'kobyashevite' 28** **'chalcanthite' 25**	**'kobyashevite' 41** **'dolerophanite' 31** **'chalcanthite' 28**	**'kobyashevite' 58** **'chalcanthite' 29** 'dolerophanite' 13	**'kobyashevite' 67** **'chalcanthite' 30** 'dolerophanite' 3	**'kobyashevite' 67** **'chalcanthite' 30** 'dolerophanite' 3	**'kobyashevite' 67** **'antlerite' 27** 'chalcanthite' 6

The amount of each phase is given in wt.%. E.s.d is ~3%. All mineral-like phases appearing during hydration/dehydration are shown in quotes. Dominating phases (≥20%) are marked in bold.

from 250°C the sample composition has reversed back to the initial chalcocyanite. The colour of the powder sample is also the initial grey (Fig. 2).

Dolerophanite $Cu_2O(SO_4)$

Hydration

The initial dolerophanite sample contained no admixtures of other phases (Fig. 3) and its powder pattern corresponds to that reported for synthetic $Cu_2O(SO_4)$ (Effenberger, 1985).

After the hydration processes have started, the phase composition undergoes significant transformations (diffraction patterns 2–4 in Fig. 3). 'Kobyashevite' $Cu_5(SO_4)_2(OH)_6{\cdot}4H_2O$ (Pekov *et al.*, 2013) and 'chalcanthite' $Cu(SO_4){\cdot}5H_2O$ (Bacon and Titterton, 1975) appear in significant amounts. The amount of dolerophanite decreases gradually, and drops down to 13 wt.% as registered in powder pattern #4.

At the next stage of hydration (diffraction patterns 5–6 in Fig. 3 and Table 1) the signature of dolerophanite has almost disappeared, and its amount is refined to yield only 3 wt.%. 'Kobyashevite' has become the major phase with 67 wt.% whereas the 'chalcanthite' content is still important with ~30 wt.%.

The last stage of the dolerophanite hydration experiment (diffraction pattern 7 in Fig. 3 and Table 1) is characterised by the almost complete disappearance of 'chalcanthite' in favour of 'antlerite', $Cu_3(SO_4)(OH)_4$ (Hawthorne *et al.*, 1989). The remains of 'chalcanthite' amount to only ~6 wt.%.

Dehydration

The dolerophanite dehydration processes with increasing temperature can be classified into three main stages (Table 2). The characteristic of stage **I** is the dominance of 'kobyashevite' although its amount gradually decreases with rising temperature. Diffraction patterns 10–12 at 75°C, 100°C and 125°C (Fig. 3) demonstrate the appearance of 'poitevinite' $Cu(SO_4){\cdot}H_2O$ (Ting *et al.*, 2009) at the expense of the 'chalcanthite'.

Dehydration stage **II**, starting at 150°C, is characterised by the complete disappearance of 'kobyashevite', with 'poitevinite' and 'antlerite' becoming the dominant phases. Minor amounts of 'chalcocyanite' (~3 wt.%) appear in the polyphasic mixture. There is a gradual decrease in the amount of 'poitevinite' with rising temperature until 300°C. The amount of 'antlerite' remains nearly constant during this process, but the amount of chalcocyanite gradually increases.

The last dehydration stage **III** starts at 325°C and is accomplished at 350°C. 'Chalcocyanite' is the dominant phase throughout this stage with ~70%. Re-appearance of 'dolerophanite' is observed at this temperature, but its amount does not exceed 20%. 'Tenorite' CuO (Brese *et al.*, 1990) is present with ~12% as an obvious product of decomposition of 'chalcocyanite' and/or 'dolerophanite'. The colour of the sample becomes brownish at the end (Fig. 3).

Alumoklyuchevskite $K_3Cu_3AlO_2(SO_4)_4$

Hydration

The initial alumoklyuchevskite sample contained no detected admixtures of other phases (Fig. 4) and its powder pattern is in a good agreement with that calculated for its recently refined crystal structure (Siidra *et al.*, 2017).

Immediately after the start of hydration, the alumoklyuchevskite sample starts to decompose and shows the diffraction pattern of two hydrated phases (diffraction patterns 2 and 3 in Fig. 4): 'cyanochroite' $K_2Cu(SO_4)_2{\cdot}6H_2O$ (Bosi *et al.*, 2009) and subordinate 'chalcanthite' $Cu(SO_4){\cdot}5H_2O$ (Bacon and Titterton, 1975). After 60 min of hydration, the reflections of alumoklyuchevskite have disappeared completely. The amount of 'cyanochroite' gradually increases, and at the end of hydration, the sample is almost completely represented by this phase (diffraction pattern 7 in Fig. 4; Table 3).

Dehydration

The dehydration behaviour of the product of the alumoklyuchevskite hydration registered by PXRD appears relatively simple. It is characterised by three main stages (Table 4). At the beginning of the experiment, when the temperature reached 25°C, the remains of 'chalcanthite' have completely disappeared and only diffraction peaks of 'cyanochroite' are present. According to the diffraction patterns 10–18 in Fig. 4, the sample undergoes gradual amorphisation.

A recrystallisation of the sample is observed in the range 300–400°C. All the observed peaks correspond to $K_2Cu(SO_4)_2$ (PDF card No. 00-017-0485, powder diffraction file from the International Centre for Diffraction Data, https://www.icdd.com/). The crystal structure of this phase is unknown. $K_2Cu(SO_4)_2$, reported recently by Zhou *et al.* (2020), has an unrelated PXRD pattern.

Note that regardless of the likely formation of a considerable amount of crystalline 'cyanochroite' during hydration, the colour of the resulting sample does not show the typical bluish tints typical for the mineral cyanochroite, but appears yellow with greenish tints instead. This might be an indication of the amorphous Al_2O_3 or its hydrated forms as decomposition products that envelop the finely dispersed crystallites of 'cyanochroite'.

Itelmenite $Na_2CuMg_2(SO_4)_4$

Hydration

The initial itelmenite sample contained no admixtures of other phases (Fig. 5) and its powder pattern is in a good agreement

https://doi.org/10.1180/mgm.2021.11 Published online by Cambridge University Press

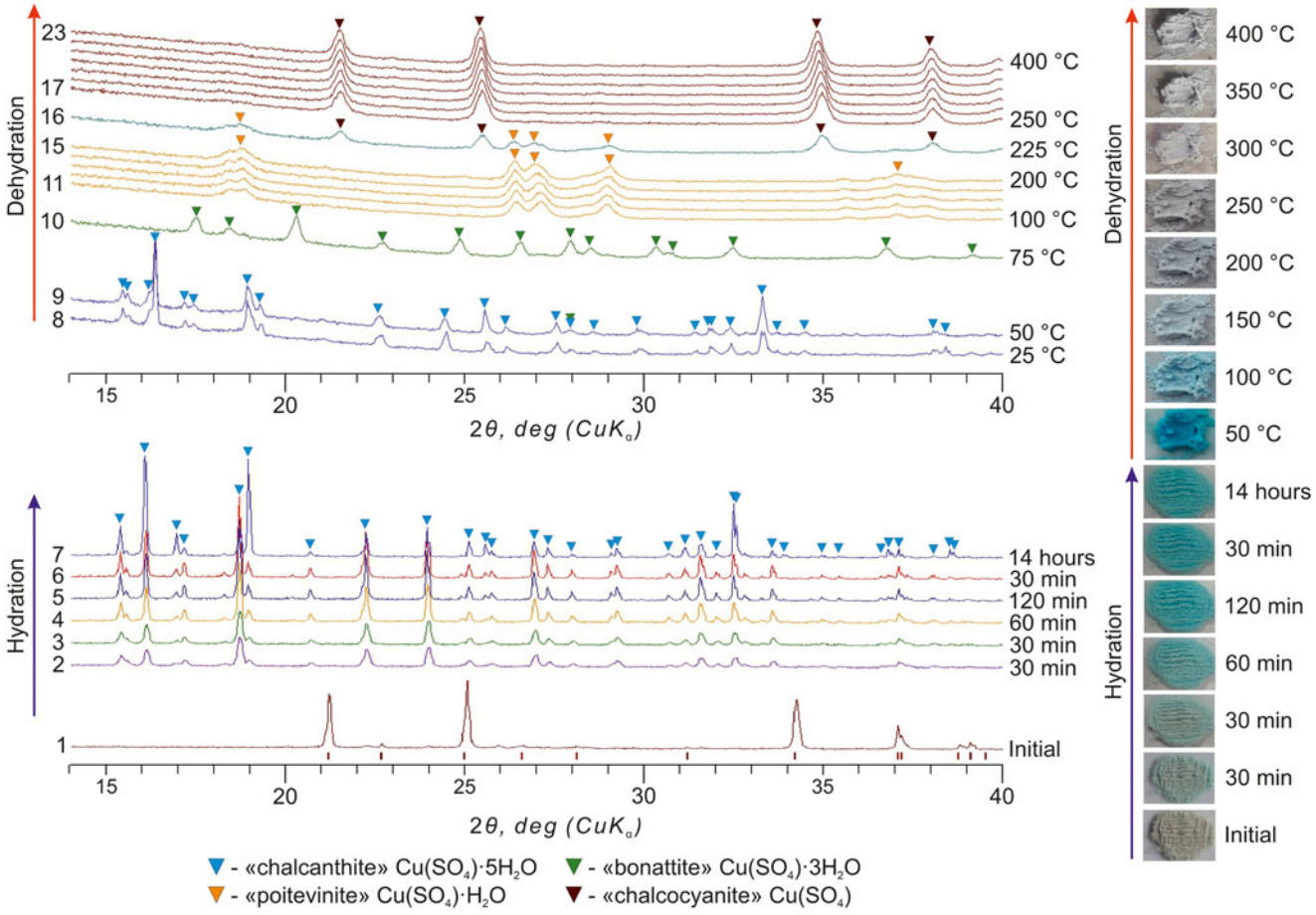

Fig. 2. XRD patterns for the products of chalcocyanite hydration (left below). Different stages of hydration are numbered on the left side. Peak positions of 'chalcanthite' $Cu(SO_4)\cdot 5H_2O$ are marked with blue triangles. XRD patterns for the products of dehydration of the mixture of hydrated sulfates initially obtained from chalcocyanite (left above). Blue – 'chalcanthite' $Cu(SO_4)\cdot 5H_2O$; green – 'bonattite' $Cu(SO_4)\cdot 3H_2O$; orange – 'poitevinite' $Cu(SO_4)\cdot H_2O$; and black – 'chalcocyanite' $Cu(SO_4)$. Hydration of chalcocyanite single-phase powder and formation of various hydrated copper sulfates is accompanied by colour changes (right). During the heating of the hydrated products the colour reverses back completely in agreement with the reversible hydration/dehydration of chalcocyanite. The relative humidity for each hydration stage is given in Table 1.

with the pattern calculated for the crystal structure of itelmenite (Nazarchuk *et al.*, 2018).

Itelmenite demonstrates remarkably complex and multiple transformations even after the first 30 min of hydration. About half of the polyphase mixture is still represented by itelmenite. The second most significant phase is 'hexahydrite' $Mg(SO_4)\cdot 6H_2O$ (Zalkin *et al.*, 1964). The other hydrates of magnesium sulfates are represented by 'pentahydrite' $MgSO_4\cdot 5H_2O$ (Baur and Rolin, 1972), 'starkeyite' $Mg(SO_4)\cdot 4H_2O$ (Baur, 1962) and 'sanderite' $Mg(SO_4)\cdot 2H_2O$ (Ma *et al.*, 2009). 'Kröhnkite' $Na_2Cu(SO_4)_2\cdot 2H_2O$ (Hawthorne and Ferguson, 1975) and 'brucite' $Mg(OH)_2$ (Mitev *et al.*, 2009) are also present in minor amounts (Table 5).

After another 30 min of hydration the amount of itelmenite is reduced. 'Kröhnkite' becomes dominant and the amount of 'hexahydrite' is reduced. New phases 'epsomite' $Mg(SO_4)\cdot 7H_2O$ (Calleri *et al.*, 1984) and 'alpersite' $(Mg,Cu)(SO_4)\cdot 7H_2O$ (Mills *et al.*, 2010) appear in minor amounts.

The third stage of hydration (diffraction patterns 4–6 in Fig. 5) is characterised by almost constant phase composition, with only slight variations in the amounts of these phases. Primary itelmenite no longer exists in the mixture, and only 'kröhnkite', 'epsomite', 'hexahydrite' and 'alpersite' are registered.

The last stage of hydration is characterised by the strong shift of the dominant phases and appearance of 'konyaite' $Na_2Mg(SO_4)_2\cdot 5H_2O$ (Mills *et al.*, 2010) in the amount of 62 wt.%.

Dehydration

At 25°C and 50°C the composition of the polyphase sample, with 'konyaite' as the dominant phase, is similar to the final stage of hydration. At 75°C the sample completely transforms into a two-phase mixture highlighting the end of the dehydration stage **I**.

Dehydration stage **II** indicates almost complete amorphisation of the sample (diffraction patterns 12–17 in Fig. 5). Some relics of crystalline matter are present, but an interpretation of the diffraction pattern is uncertain.

Dehydration stage **III** is characterised by the presence of anhydrous crystalline phases only. Simple $Mg(SO_4)$ (Rentzeperis and Soldatos, 1958) is the dominant phase in the range from 275°C to 375°C. Its amount gradually reduces with the rise of the temperature in favour of the amount of 'chalcocyanite' $Cu(SO_4)$. By 275°C itelmenite has already reappeared in minor amounts and becomes the

https://doi.org/10.1180/mgm.2021.11 Published online by Cambridge University Press

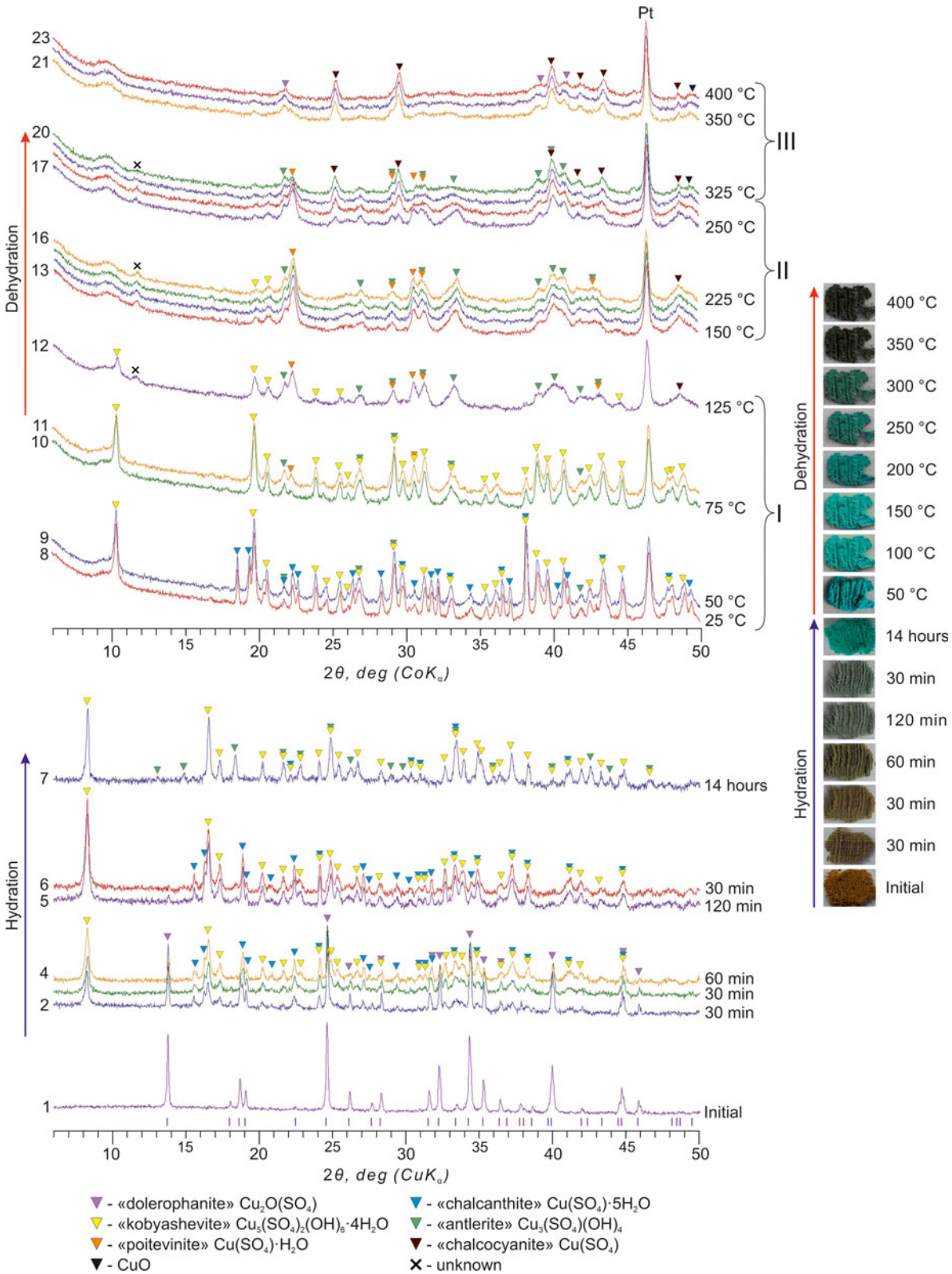

Fig. 3. XRD patterns for the products of dolerophanite hydration (left below). Different stages of hydration are numbered on the left side. XRD patterns for the products of dehydration of the mixture of hydrated sulfates initially obtained from dolerophanite (left above). Different stages of dehydration are numbered on the left side. Hydration of dolerophanite single-phase powder and formation of various hydrated copper sulfates is accompanied by colour changes (right). During the heating of the hydrated products the colour reverses back in agreement with the formation of a mixture of anhydrous sulfates. The relative humidity for each hydration stage is given in Table 1.

https://doi.org/10.1180/mgm.2021.11 Published online by Cambridge University Press

dominant phase at 400°C. 'Vanthoffite' $Na_6Mg(SO_4)_4$ (Fischer and Hellner, 1964), 'metathénardite' $Na_2(SO_4)$ (Rasmussen *et al.*, 1996) and MgO (Fan *et al.*, 2008) are minor phases.

In the photographs (Fig. 5), it is clearly seen that the initial grey colour of the itelmenite powder sample fades away towards the end of the experiment and becomes light grey.

Discussion

Chemistry

Chalcocyanite

The reversible hydration of this mineral has been studied previously using synchrotron radiation (Ting *et al.*, 2009). The good agreement of our results with those reported by (Ting *et al.*, 2009) makes us confident that our experimental setup reproduces the hydration process of this mineral sufficiently well. Thus, chalcocyanite can be relied on as a reference system for the other minerals studied in this work. Under high RH (relative humidity) at ambient conditions, hydration proceeds in one step yielding the thermodynamically stable product, i.e. chalcanthite. The small amount of chalcocyanite remaining even after several hours of hydration can be probably explained by formation of chalcanthite 'shells' around the initial chalcocyanite particles, which block or strongly retard the hydration process. On heating, formation of the less water-rich forms proceeds in the temperature intervals, which agree well with the data of Cheng *et al.* (2019). Note the relatively low crystallinity of the monohydrate.

Dolerophanite

Hydration: This case is more complex than chalcocyanite as the hydration involves formation of basic copper sulfates whose interconversion depends on a variety of external conditions including temperature, presence of liquid phase and its acidity as well as copper concentration (Yoder *et al.*, 2007; Stanimirova and Ivanova, 2019). The first step of hydration can be described tentatively by an equation $3Cu_2O(SO_4) + 14H_2O = Cu_5(SO_4)_2(OH)_6{\cdot}4H_2O + Cu(SO_4){\cdot}5H_2O$, or expressed in shorthand by the Cu:SO_4 ratio, 3 (2:1) = (1:1) + (5:2). The (5:2) compound is known to be easily formed either by reaction of CuO with an aqueous solution of $CuSO_4$ (Stanimirova and Ivanova, 2019) or gently increasing the pH of a $CuSO_4$ solution by adding small amounts of alkalis (Yoder *et al.*, 2007), probably due to kinetic reasons. It was found to be stable in contact with aqueous solutions of cupric sulfate (1M or slightly below), while in pure water it readily converts into brochantite (4:1) or its hydrates (posnjakite and langite). In addition, Yoder *et al.* (2007) note that in their experiments, antlerite (3:1) could only be obtained at 80°C or above. Yet, in our case kobyashevite, as the major hydration product of dolerophanite, was in steady contact with a slurry containing solid chalcanthite, i.e. copper sulfate pentahydrate, during the hydration process. Note that Yoder *et al.* (2007) studied the stability of kobyashevite only against 1M $Cu(SO_4)$ and pure water; other concentrations of cupric sulfate solution may already lead to formation of antlerite at room temperature. Further investigations of basic copper sulfate interconversions in copper sulfate solutions of varied concentrations, including the presence of solid $Cu(SO_4){\cdot}5H_2O$, are obviously necessary to provide better understanding of these processes.

Formation of synthetic kobyashevite was also detected upon hydration of a more complex copper oxysulfate mineral, euchlorine $KNaCu_3O(SO_4)_2$ (Siidra *et al.*, 2019a), but formation of antlerite was not observed. Possibly, the concentration of copper sulfate in the slurries formed was not high enough because of the relatively low solubility of kröhnkite-type double copper–alkali sulfate products.

Dehydration: Evaporation of water from the initial slurry results in the initial crystallisation of dissolved chalcanthite. In agreement with Yoder *et al.* (2007), the antlerite content increases as the temperature rises and water-rich kobyashevite dehydrates. This step can be described by a tentative equation $2Cu_5(SO_4)_2(OH)_6{\cdot}4H_2O = 3Cu_3(SO_4)(OH)_4 + Cu(SO_4){\cdot}H_2O + 7H_2O$, or in shorthand, 2(5:2) = 3(3:1) + (1:1). Poitevinite is also formed by dehydration of chalcanthite. At the final steps, copper hydroxyl sulfates decompose with loss of water and formation of cyanochroite and tenorite. We note that, while our study was restricted to 450°C, the suggested deposition temperature on the wall of the fumarole, only a small part of the initial dolerophanite was recovered. In thermoanalytical studies dedicated to dehydration of basic copper sulfates (Ramamurthy and Secco, 1970; Uzunov *et al.*, 1995; Tanaka and Koga 1988), thermal effects attributed to the formation of synthetic dolerophanite (in a CuO-rich mixture) are reported to occur at somewhat higher temperatures (~500°C). In one of our test experiments in a sealed silica tube no reaction was observed between CuO and $Cu(SO_4)$ up to 550°C. In contrast, formation of basic copper alkali sulfates proceeds easily below 450°C both upon dehydration (Siidra *et al.*, 2019a) and *in silico*.

Alumoklyuchevskite

The chemical identity of at least some of the hydration products remains obscure due to their amorphous nature. Based on the crystalline products formed at the first stage, we suggest the following equation: $2K_3Cu_3AlO_2(SO_4)_4 + (26 + x)H_2O = 3K_2Cu(SO_4)_2{\cdot}6H_2O + Cu(SO_4){\cdot}5H_2O + [Al_2(SO_4)(OH)_4{\cdot}xH_2O]$, the amorphous part (with a tentative composition) shown in brackets. The low temperature of the hydration process probably favours formation of amorphous basic aluminium salts that crystallise with difficulty, as noted particularly for sulfates (Nordstrom, 1982). It is possible that the progressive disappearance of chalcanthite is caused by its slow dissolution in the slurry (it is more water soluble compared to cyanochroite) and sorption by the aluminium-based amorphous phase. Further reactions involving formation of amorphous double copper–aluminium hydroxysulfates are also possible.

Upon heating, given the overall cation ratio, one could expect formation of sulfates with a K:Cu ratio of 1:1, i.e. $K_2Cu_2(SO_4)_3$ (Lander *et al.*, 2017), or a mixture of $K_2Cu(SO_4)_2$ and $Cu(SO_4)$. Instead, the only process detectable by PXRD study is dehydration of cyanochroite, also via an amorphous precursor. Thermogravimetry and differential thermal analysis (TG/DTA) studies of synthetic cyanochroite (Nagase *et al.*, 1978) revealed a two-step loss of water (which is complete below 150°C) followed by two endothermal effects at 370 and 520°C, the latter being attributed to melting. The data provided in PDF card No. 00-017-0485 is not yet interpreted, but refers to the compound prepared by dehydration of cyanochroite, most likely to the high-temperature form of $K_2Cu(SO_4)_2$ while the structure reported by Zhou *et al.* (2020) refers to its low-temperature form, according to the method of preparation. In our experiment, crystallisation of the high-temperature form starts from ~275°C, which might be enhanced by the amorphous nature of the precursor or by the presence of aluminium. Detailed temperature-dependent studies of $K_2Cu(SO_4)_2{\cdot}6H_2O$ and its anhydrous form, particularly DTA/PXRD, are evidently necessary to confirm the nature of compound noted in PDF card No. 00-017-0485.

https://doi.org/10.1180/mgm.2021.11 Published online by Cambridge University Press

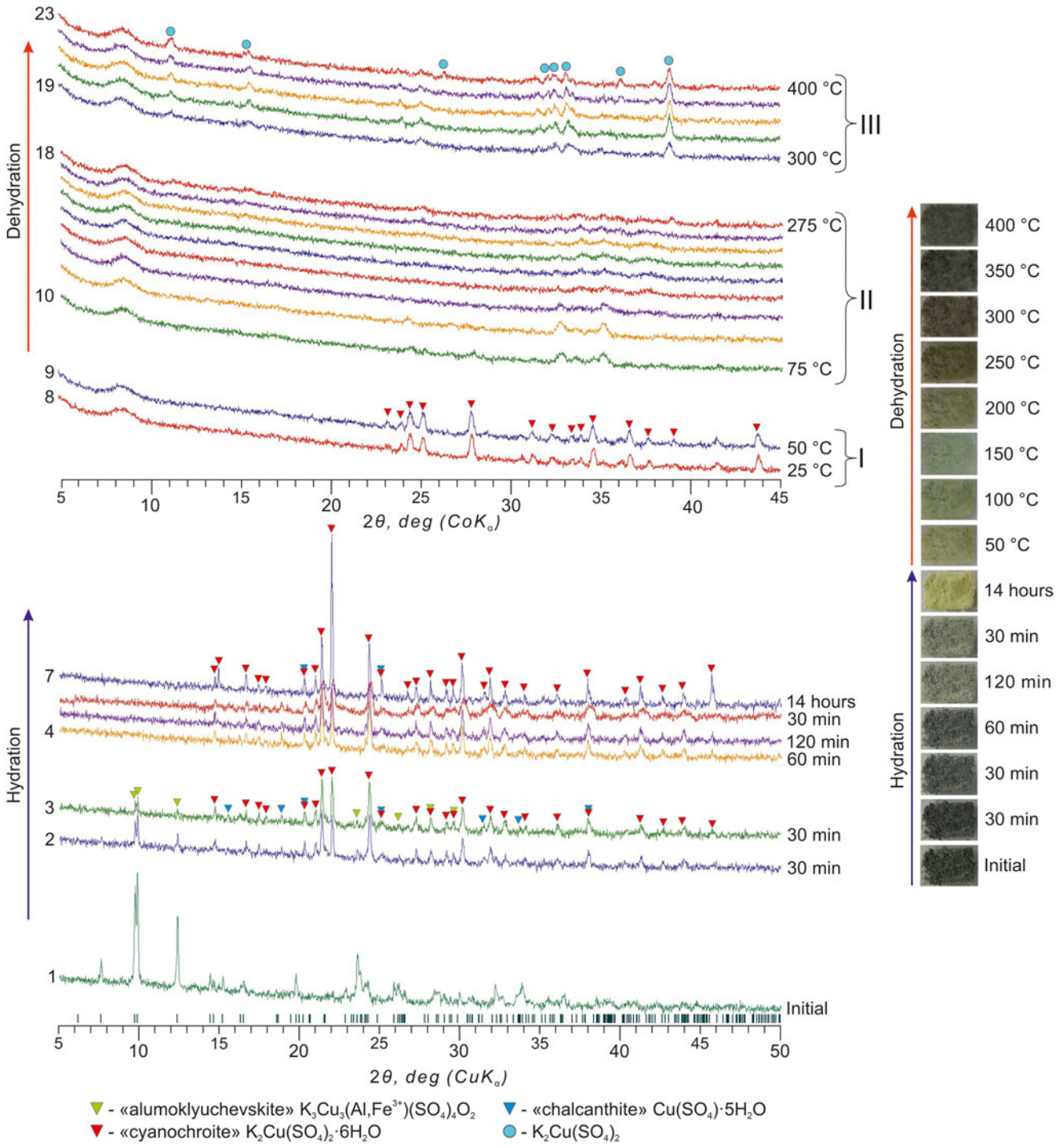

Fig. 4. XRD patterns for the products of alumoklyuchevskite hydration (left below). Different stages of hydration are numbered on the left side. XRD patterns for the products of dehydration of the mixture of hydrated sulfates initially obtained from alumoklyuchevskite (left above). Different stages of dehydration are numbered on the left side. Hydration of alumoklyuchevskite single-phase powder and formation of various hydrated copper sulfates is accompanied by the colour changes (right). During the heating of the mixture the colour partially reverses back. The relative humidity for each hydration stage is given in Table 3.

Itelmenite

Due to the absence of additional oxygen atoms, the formation of any basic salts upon hydration is not expected. Only a few selected and partial studies have been performed within the relatively complex $Na_2(SO_4)$–$Cu(SO_4)$–$Mg(SO_4)$–H_2O system (e.g. Steiger *et al.*, 2011; Lindström *et al.*, 2016). In addition, rapid hydration is most likely driven by kinetic factors, i.e. compounds more easily formed are observed first. Hence, the initial hydration stage can be described by the following tentative equation: $Na_2CuMg_2(SO_4)_4 + (2 + 2x)H_2O = Na_2Cu(SO_4)_2{\cdot}2H_2O + 2(Mg, Cu)(SO_4){\cdot}xH_2O$. The latter formula designates the successively formed magnesium sulfates that may also accommodate the

https://doi.org/10.1180/mgm.2021.11 Published online by Cambridge University Press

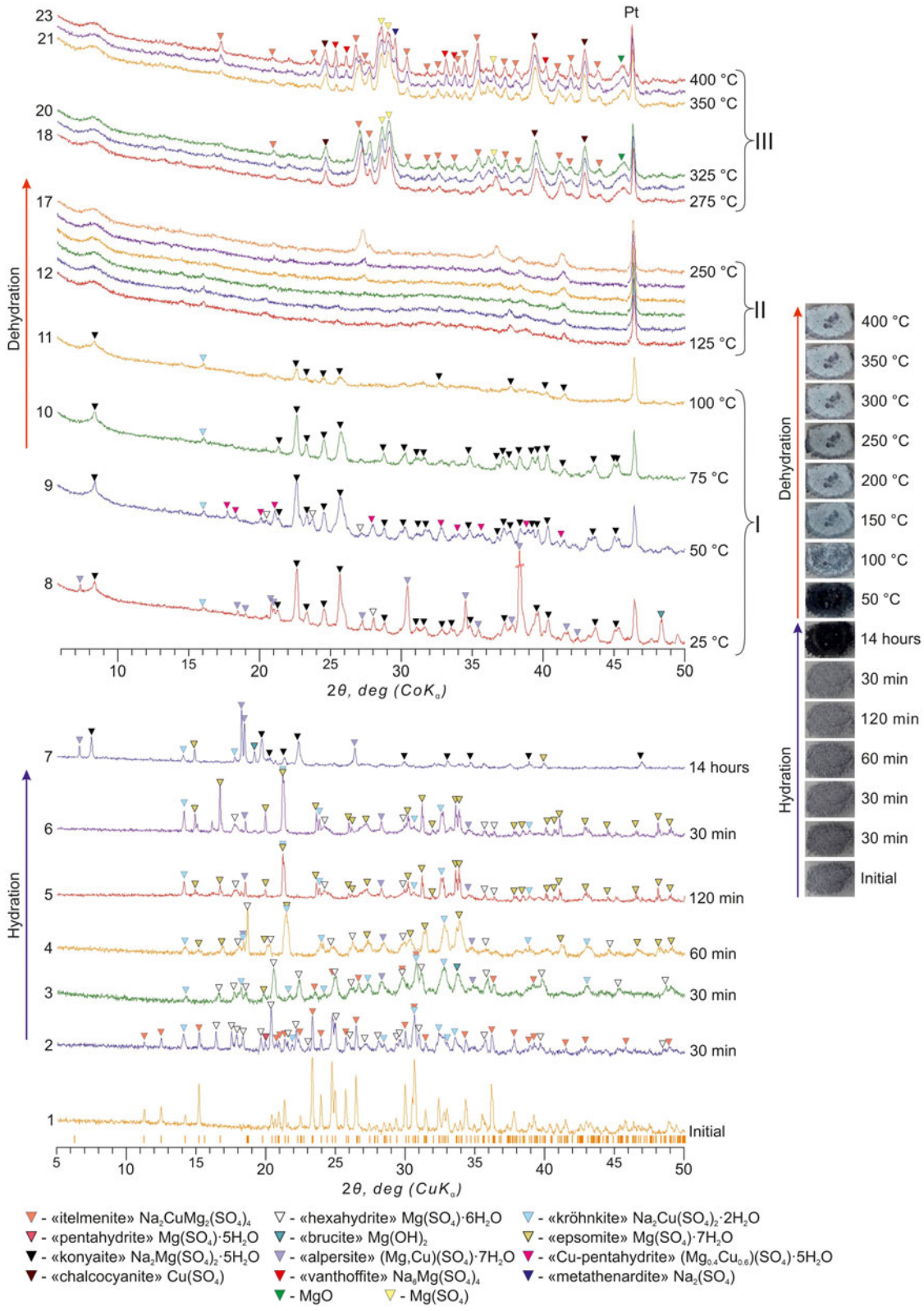

Fig. 5. XRD patterns for the products of itelmenite hydration (left below). Different stages of hydration are numbered on the left side. XRD patterns for the products of dehydration of the mixture of hydrated sulfates initially obtained from itelmenite (left above). Different stages of dehydration are numbered on the left side. Hydration of itelmenite single-phase powder and formation of various hydrated copper and magnesium sulfates is accompanied by the colour changes (right). During the heating of the mixture the colour reverses back. The relative humidity for each hydration stage is given in Table 5.

https://doi.org/10.1180/mgm.2021.11 Published online by Cambridge University Press

Table 2. Evolution of the mixture of hydrated sulfate phases, formed as a result of dolerophanite hydration, upon heating.

I						II			
+25	+50	+75	+100	+125		+150	+175	+200	
'kobyashevite' 63 **'chalcanthite' 29** 'antlerite' 8	**'kobyashevite' 62** **'chalcanthite' 29** 'antlerite' 9	**'kobyashevite' 73** 'poitevinite' 17 'antlerite' 10	**'kobyashevite' 68** **'poitevinite' 22** 'antlerite' 10	**'kobyashevite' 49** **'poitevinite' 39** 'antlerite' 10 'chalcocyanite' 2		**'poitevinite' 67** **'antlerite' 27** 'chalcocyanite' 3 'kobyashevite' 3	**'poitevinite' 69** **'antlerite' 27** 'chalcocyanite' 2 'kobyashevite' 2	**'poitevinite' 67** **'antlerite' 28** 'chalcocyanite' 3 'kobyashevite' 2	
II					III				
+225	+250	+275	+300	+325		+350	+375	+400	
'poitevinite' 63 **'antlerite' 31** 'chalcocyanite' 5 'kobyashevite' 1	**'poitevinite' 49** **'antlerite' 33** 'chalcocyanite' 18	**'poitevinite' 39** **'antlerite' 32** **'chalcocyanite' 29**	**'poitevinite' 38** **'antlerite' 33** **'chalcocyanite' 29**	**'chalcocyanite' 40** **'antlerite' 29** **'poitevinite' 29** 'tenorite' 2		**'chalcocyanite' 68** **'dolerophanite' 20** 'tenorite' 12	**'chalcocyanite' 69** 'dolerophanite' 19 'tenorite' 12	**'chalcocyanite' 69** 'dolerophanite' 18 'tenorite' 13	

The amount of each phase is given in wt.%. E.s.d is ~3%. All mineral-like phases appearing during hydration/dehydration are shown in quotes. Dominating phases (≥20%) are marked in bold.

remaining copper sulfate as the latter's hydrates are not observed. The following steps correspond mostly to progressive hydration of Mg/Cu sulfates until the point where the largest hydration point is observed (epsomite and alpersite). Further reactions are likely to proceed in partially deliquesced samples: dissolution of kröhnkite and epsomite leads to formation of konyaite; the released cupric sulfate contributes to alpersite that also forms at the expense of epsomite: $Na_2Cu(SO_4)_2{\cdot}2H_2O + 3Mg(SO_4){\cdot}7H_2O + 3H_2O = Na_2Mg(SO_4)_2{\cdot}5H_2O + 3Mg_{0.67}Cu_{0.33}(SO_4){\cdot}7H_2O$. This reaction is partially reversed on heating when water starts to evaporate. Partial dehydration of alpersite also contributes to the transient Cu-rich pentahydrite. As in the previous case, decomposition of the complex mixture of hydrates results in amorphisation (partial dissolution?). It is therefore not possible to trace the origin of crystalline phases arising at ~275°C. The last step is characterised by a slow reaction of anhydrous sulfates with formation of the initial itelmenite, probably enhanced by the seed crystals formed from the amorphous precursor. The small amount of $Mg(OH)_2$ formed due to partial hydrolysis converts independently into MgO.

Structural evolution

Analysis of the sequential phase formation shows that the behaviour of the studied minerals differs significantly (Figs 6, 7). The formulas and structures of hydrates, formed as a result of chalcocyanite transformations during hydration and subsequent heating, are more complex than the initial simple copper sulfate $Cu(SO_4)$. The opposite behaviour, namely the formation of simpler phases during hydration, was described recently in our investigation of euchlorine (Siidra *et al.*, 2019a). To analyse quantitatively the sequence of transformations of mineral phases, we performed an analysis of their structural complexity, I_G in bits/atom, using the approach proposed in Krivovichev (2013). Additionally, for each of the minerals, weighted average values of I_G bits/atom at each stage of the experiment were calculated (Fig. 6, 7), using the molar fraction of each mineral phase (where x_i – molar fraction, w_i – weight % and M_i – molar mass, of the i phase, respectively).

In the case of chalcocyanite (2.252 bits/atom) (Fig. 6a) and dolerophanite (2.750 bits/atom) (Fig. 6b), the complexity increases due to the fact that even the simple hydrated offspring have a higher structural complexity than their anhydrous analogues. This is in agreement with a common structural trend (Krivovichev, 2014). Illustrative examples are anhydrite $Ca(SO_4)$ (1.918 bits/atom) and gypsum $Ca(SO_4){\cdot}2H_2O$ (2.752 bits/atom).

The structural complexity of the phases (cyanochroite and chalcanthite) formed during hydration of the alumoklyuchevskite (Fig. 6c) is lower than that of the initial mineral. As noted above, there are currently no structural data on the '$K_2Cu(SO_4)_2$' phase (PDF card No. 00-017-0485) available, thus the structural complexity could not be estimated for the final stage.

In an experiment with itelmenite, the weighted average structural complexity of the phases formed also decreases, however, by the end of dehydration, having passed through the amorphous state stage, when anhydrous sulfates are formed at high temperatures, its value increases again (Fig. 7a).

The phases resulting from hydration and subsequent dehydration of euchlorine (Fig. 7b) demonstrate a significant reduction in structural complexity with respect to the initial phase. However, by the end of the experiment, as the phase composition of the

https://doi.org/10.1180/mgm.2021.11 Published online by Cambridge University Press

Table 3. Evolution of primary alumoklyuchevskite into mixtures of hydrated sulfates during the hydration experiments at 23°C, different duration and different relative humidity.

Initial sample Stage 1	Stage 2 30 min, humidity 85%	Stage 3 30 min, humidity 86%	Stage 4 60 min, humidity 88%	Stage 5 120 min, humidity 90%	Stage 6 30 min, humidity 91%	Stage 7 14 hours, humidity 94%
alumoklyuchevskite 100	**'cyanochroite' 82** 'alumoklyuchevskite' 13 'chalcanthite' 5	**'cyanochroite' 86** 'chalcanthite' 9 'alumoklyuchevskite' 5	**'cyanochroite' 89** 'chalcanthite' 11	**'cyanochroite' 90** 'chalcanthite' 10	**'cyanochroite' 81** 'chalcanthite' 19	**'cyanochroite' 98** 'chalcanthite' 2

The amount of each phase is given in wt.%. E.s.d is ~3%. All mineral-like phases appearing during hydration/dehydration are shown in quotes. Dominating phases (≥20%) are marked in bold.

Table 4. Evolution of the mixture of hydrated sulfate phases, formed as a result of alumoklyuchevskite hydration, upon heating. Dominating phases (≥20%) are marked in bold. The transformation can be subdivided into three main stages (**I**–**III**) in accordance with the dominance of different phases (marked in bold). Amount of each phase is given in wt. %. E.s.d is ~3%.

I		II								III				
+25	+50	+75	+100	+125	+150	+175	+200	+225	+250	+275	+300	+325	+350	+375	+400
'cyanochroite' 100	**'cyanochroite' 100**	**Amorphisation**									**'$K_2Cu(SO_4)_2$' 100**				

The amount of each phase is given in wt.%. E.s.d is ~3%. All mineral-like phases appearing during hydration/dehydration are shown in quotes. Dominating phases (≥20%) are marked in bold.

Table 5. Evolution of primary itelmenite into mixtures of hydrated sulfates during the hydration experiments at 23°C, different duration and different relative humidity.

Initial sample Stage 1	Stage 2 30 min, humidity 85%	Stage 3 30 min, humidity 86%	Stage 4 60 min, humidity 88%	Stage 5 120 min, humidity 90%	Stage 6 30 min, humidity 91%	Stage 7 14 hours, humidity 94%
itelmenite 100	**'itelmenite' 48** **'hexahydrite' 35** 'kröhnkite' 8 'pentahydrite' 3 'sanderite' 3 'starkeyite' 2 'brucite' 1	**'kröhnkite' 34** **'itelmenite' 31** **'hexahydrite' 24** 'alpersite' 6 'brucite' 3 'epsomite' 2	**'epsomite' 66** **'kröhnkite' 24** 'hexahydrite' 7 'alpersite' 3	**'kröhnkite' 46** **'epsomite' 42** 'hexahydrite' 9 'alpersite' 3	**'epsomite' 52** **'kröhnkite' 44** 'hexahydrite' 2 'alpersite' 2	**'konyaite' 62** **'alpersite' 31** 'kröhnkite' 3 'epsomite' 3 'brucite' 1

The amount of each phase is given in wt.%. E.s.d is ~3%. All mineral-like phases appearing during hydration/dehydration are shown in quotes. Dominating phases (≥20%) are marked in bold.

sample returns to the initial, almost single-phase euchlorine composition, the weighted average structural complexity becomes close to the initial value.

Thus, the performed analysis shows that many of the primary exhalative Cu^{2+}-containing sulfates are structurally of intermediate complexity (Krivovichev, 2013). Alumoklyuchevskite (4.892 bits/atom), itelmenite (4.644 bits/atom), the previously studied euchlorine (4.440 bits/atom) (Siidra *et al.*, 2019a) (Figs 6, 7) and saranchinaite (5.700 bits/atom) (Siidra *et al.*, 2018a) are much more structurally complex than the products of their hydration. Despite the decrease in the structural complexity for the complex anhydrous sulfates during hydration, with subsequent heating and dehydration, the complexity increases again and almost reaches its initial values. It is worth noting that the rock-forming minerals of the scoria (Fedotov and Markhinin, 1983) are structurally simple (labradorite 3.700 bits/atom, diopside 2.522 bits/atom, olivine 2.522 bits/atom, chromite 1.379 bits/atom).

Changes in coordination of Cu^{2+} cations as a result of hydration/dehydration processes also demonstrate a number of interesting patterns. The types of coordination polyhedra of copper in the structure of each of the minerals or mineral phases, identified during the experiments, are sketched on the left side of Figs 6 and 7. All of the Cu–O bonds <3Å were taken into consideration. For the considered anhydrous copper sulfate minerals (and, in general, for other known fumarolic copper sulfates), the following coordination environments are characteristic: square pyramid CuO_5 with different degrees of distortion and octahedron CuO_6. A typical structural characteristic of several anhydrous copper sulfate minerals of fumarolic origin (dolerophanite, euchlorine, alumoklyuchevskite and wulffite), is the presence of oxocentred OCu_4 tetrahedra. These are absent in the structures of all known hydrated minerals or synthetic compounds of the class under consideration. During the transformation to hydrated species (the diversity of which is much greater than that of anhydrous sulfates), a general pattern manifests itself – this is the formation of [4+2] $CuO_n(H_2O)_m(OH)_k$ octahedra (Table 7) with different degrees of distortion (Figs 6, 7) due to the Jahn–Teller effect. A few exceptions from the [4+2] coordination environments and formation of a [4+1+1] coordination are found in the cases of itelmenite and wulffite. CuO_4OO [4+1+1] strongly distorted polyhedra are observed in both minerals. The coordination environment of Cu^{2+} cations is represented by the three types of ligands, *viz.* O atoms, OH groups and H_2O molecules.

https://doi.org/10.1180/mgm.2021.11 Published online by Cambridge University Press

Table 6. Evolution of the mixture of hydrated sulfate phases, formed as a result of itelmenite hydration, upon heating. The evolution can be subdivided into three main stages (I–III) in accordance with the dominance of different phases.

I				II					
+25	+50	+75	+100	+125	+150	+175	+200	+225	+250
'konyaite' 68 **'alpersite' 29** 'brucite' 2 'epsomite' 1	**'konyaite' 68** 'Cu-pentahydrite' 19 'hexahydrite' 8 'kröhnkite' 5	**'kröhnkite' 90** 'konyaite' 10	**'kröhnkite' 75** **'konyaite' 25**	**Amorphisation**					

III					
+275	+300	+325	+350	+375	+400
$MgSO_4$ 70 **'chalcocyanite' 23** 'itelmenite' 6 MgO 1	**$MgSO_4$ 69** **'chalcocyanite' 23** 'itelmenite' 7 MgO 1	**$MgSO_4$ 50** **'chalcocyanite' 29** 'itelmenite' 16 MgO 2 'vanthoffite' 2 'metathenardite' 1	**$MgSO_4$ 45** **'itelmenite' 29** **'chalcocyanite' 21** MgO 2 'vanthoffite' 2 'metathenardite' 1	**$MgSO_4$ 39** **'itelmenite' 35** 'chalcocyanite' 16 'vanthoffite' 7 MgO 2 'metathenardite' 1	**'itelmenite' 38** **$MgSO_4$ 37** 'chalcocyanite' 13 'vanthoffite' 10 MgO 1 'metathenardite' 1

The amount of each phase is given in wt.%. E.s.d is ~3%. All mineral-like phases appearing during hydration/dehydration are shown in quotes. Dominating phases (≥20%) are marked in bold.

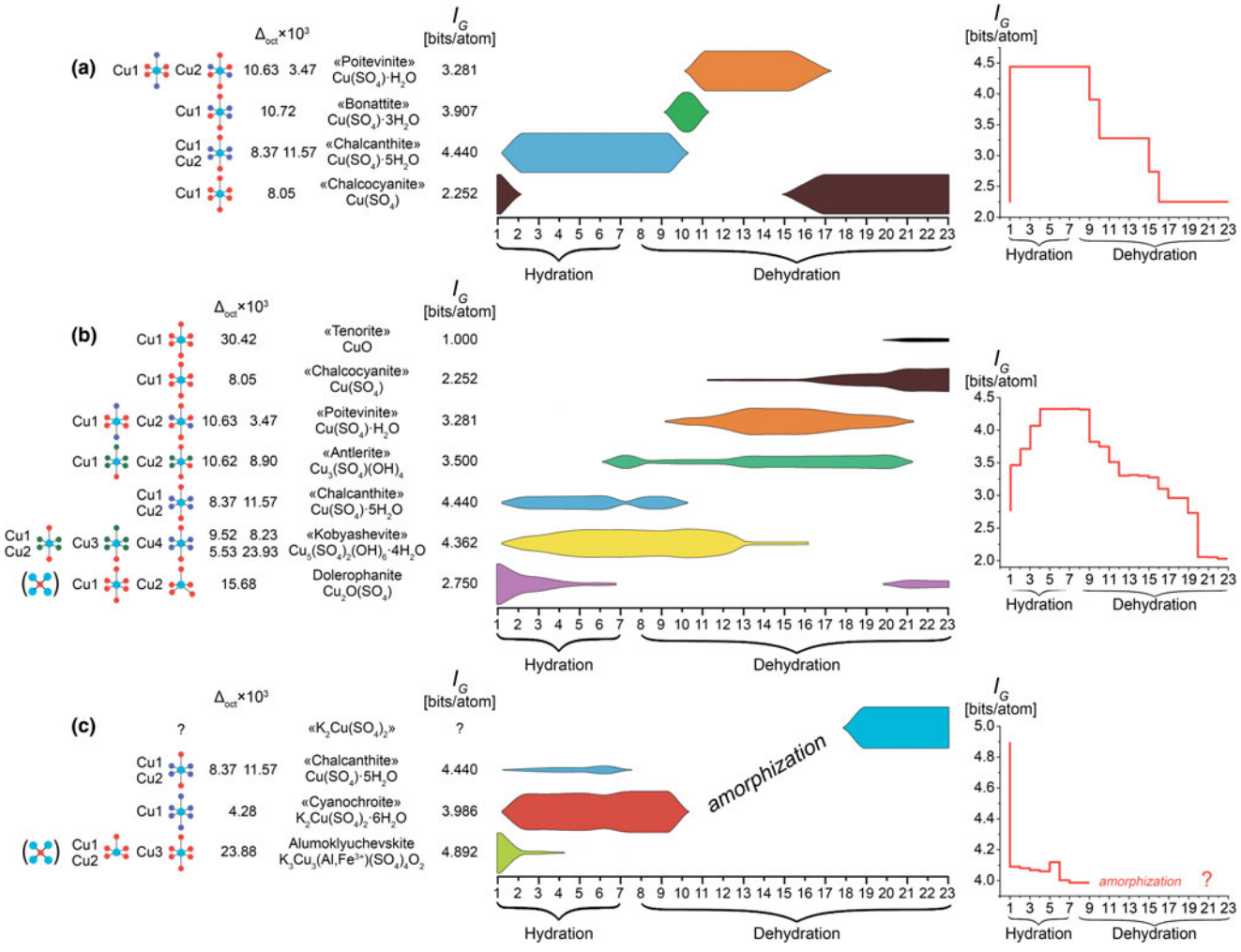

Fig. 6. General schemes of the evolution of chalcocyanite (a), dolerophanite (b) and alumoklyuchevskite (c) during the different stages of hydration and dehydration. Evolution of the structural complexity (weighted average values of I_G bits/atom) is shown on the right hand side. I_G bits/atom and types of $CuO_x(H_2O)_n(OH)_m$ polyhedra (Cu^{2+} = light blue, O^{2-} = red, H_2O = blue and OH^- = green) in the structure for each mineral phase are shown to the left. ×10^3 bond-length distortion parameter for each Cu-centred octahedron is given.

https://doi.org/10.1180/mgm.2021.11 Published online by Cambridge University Press

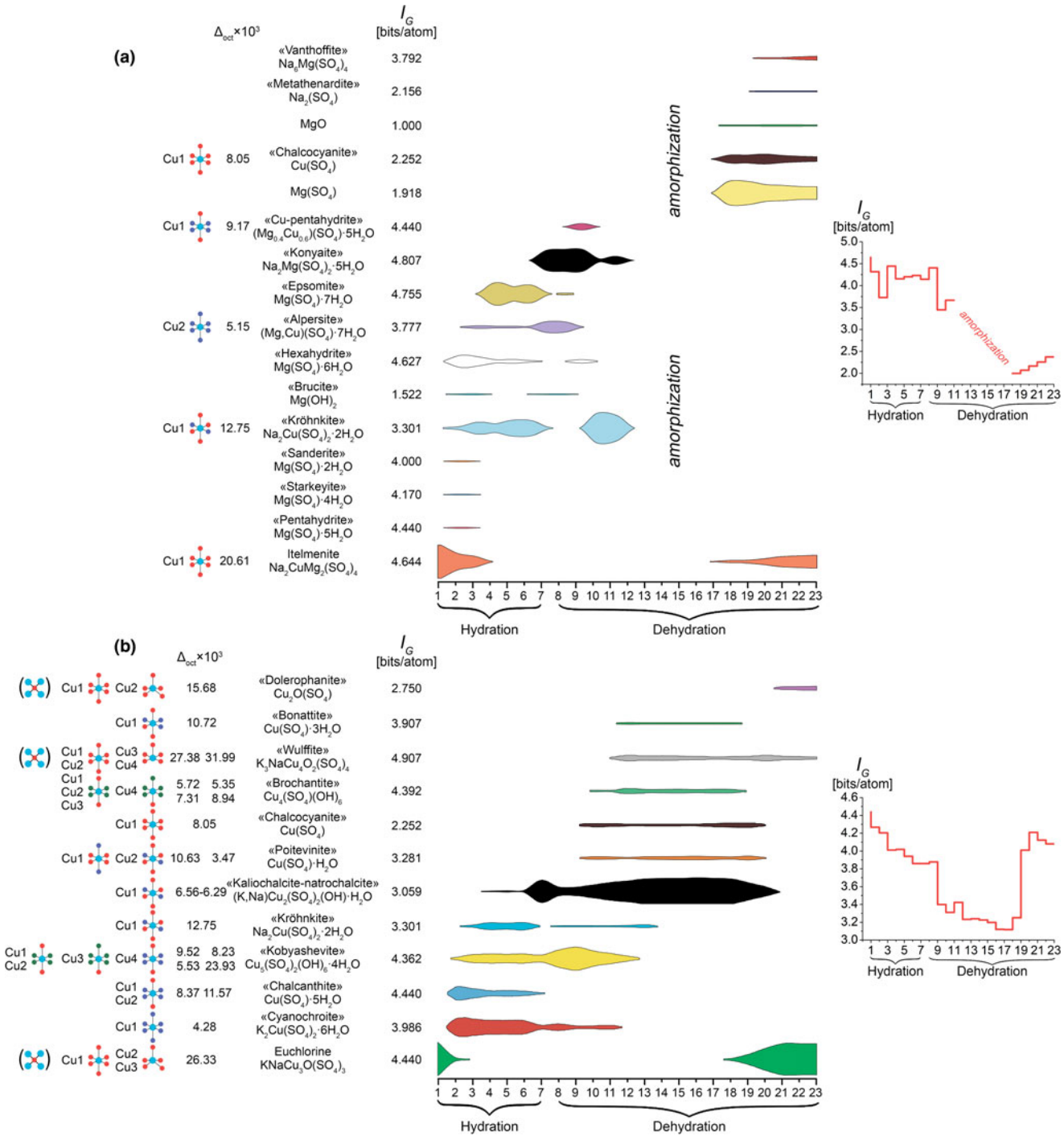

Fig. 7. General schemes of the evolution of itelmenite (a) and euchlorine (after Siidra *et al.*, 2019a) (b) during the different stages of hydration and dehydration. Evolution of the structural complexity (weighted average values of I_G bits/atom) is shown to the right. I_G bits/atom and types of $CuO_x(H_2O)_n(OH)_m$ polyhedra (Cu^{2+} = light blue, O^{2-} = red, H_2O = blue and OH^- = green) in the structure for each mineral phase are shown to the left. ×10^3 bond-length distortion parameter for each Cu-centred octahedron is given.

The following Δ_{oct} bond-length distortion parameter, suggested in Wildner (1992), was used for octahedrally coordinated *M* sites in all mineral phases listed in Figs 6 and 7: $\Delta_{oct} = \frac{1}{6}\sum_{i=1}^{6}\left[\frac{(d_i - d_m)}{d_m}\right]^2$, where d_i = (Cu–O) bond length and d_m = <Cu–O> bond length. As can be seen, the values of $\Delta_{oct}\times10^3$ are higher for non-protonated CuO_6 octahedra in anhydrous sulfate structures, while for octahedra with the presence of OH groups and H_2O molecules in the coordination of the Cu^{2+} cation, the values are lower. An exception is the $Cu4(H_2O)_4O_2$ octahedron in the kobyashevite structure, showing the distortion value $\Delta_{oct}\times10^3$ = 23.93. Conversely, the CuO_6 octahedron in the structure of chalcocyanite has a low $\Delta_{oct}\times10^3$ value of 8.05. If we exclude these two octahedra from the calculation, then the average $<\Delta_{oct}\times10^3>$ for the protonated octahedra in the structures of the considered

https://doi.org/10.1180/mgm.2021.11 Published online by Cambridge University Press

Table 7. Minimum, maximum and average equatorial and apical Cu–O bond-length values in $CuO_x(H_2O)_n(OH)_m$ octahedra in the structures of mineral phases listed in Figs 6 and 7 and Tables S1 and S2 (Supplementary material, see below).

Anhydrous species				Hydrated species											
Cu–O_{eq}		Cu–O_{ap}		Cu–O_{eq}		Cu–O_{ap}		Cu–OH_{eq}		Cu–OH_{ap}		Cu–H_2O_{eq}		Cu–H_2O_{ap}	
min	1.882	min	2.153	min	1.942	min	2.293	min	1.907	min	2.260	min	1.885	min	2.279
max	2.070	max	2.885	max	2.034	max	2.660	max	2.100	max	2.363	max	2.103	max	2.418
<Cu–O_{eq}>	1.964	<Cu–O_{ap}>	2.623	<Cu–O_{eq}>	1.974	<Cu–O_{ap}>	2.410	<Cu–OH_{eq}>	1.987	<Cu–OH_{ap}>	2.305	<Cu–H_2O_{eq}>	1.994	<Cu–H_2O_{ap}>	2.341

mineral phases is 8.03, while for anhydrous it is several times higher at 25.18.

The crystal chemistry of divalent copper cations in oxysalts is determined by the Jahn–Teller effect and is responsible for the variety of structures and transformation processes during hydration processes. The pronounced Jahn–Teller effect and low crystal field stabilisation energy for the $3d^9$ configuration makes the coordination sphere of Cu^{2+} particularly non-rigid that enhances these transformations and contributes to structural diversity. Copper polyhedra shown in Figs 6 and 7 show that during the hydration processes, protonated oxygen atoms generally occupy the equatorial plane, while the apical atoms remain involved in the bonding with sulfate tetrahedra.

Another interesting observation is the pattern of the significantly more complex behaviour of fumarolic minerals, as exemplified by dolerophanite, with additional oxygen atoms in its composition (Krivovichev *et al.*, 2013). Overall, the crystal chemistry of hydroxysalts is essentially richer due to greater variability of polymeric *M*–OH architectures as negatively charged hydroxyl groups can bridge several *M* cations, which is uncommon for neutral water ligands. Therefore, hydration of minerals initially containing O^{2-} anions as parts of oxocomplexes (euchlorine and dolerophanite), proceeds with sequential formation of a large series of hydroxysalts. Formation of several successive hydrated hydroxysalts reflects an evident competition between charged hydroxyl and neutral, but more abundant water molecules as ligands. The family of basic copper sulfates, anhydrous and hydrated, is relatively rich; our results, as compared to reference data, indicate that their interconversions are far from being studied in detail. This suggests that, on the one hand, this family will very likely be enriched upon further experimental studies; on the other hand, some more basic copper sulfates, known as synthetic species only, may be found in nature, particularly if sampling is deliberately performed in 'wet' seasons.

On the contrary, hydration of itelmenite with a relatively complex 'initial' structure without additional oxygen atoms, which are strong Lewis bases, results in formation of simpler hydrates. The lower the temperature and the larger the excess of water, the higher hydration numbers are observed for cations. Ultimately, the more abundant water molecules expel the bridging sulfate anions from the metal coordination sphere yielding relatively simple fully hydrated structures.

Concluding remarks

A study of the evolution of sulfates in hydration and dehydration processes has demonstrated the complexity of the processes for a number of minerals. The temperature regime on the active fumaroles of the scoria cones of the Tolbachik volcano is not constant and changes even over relatively short periods of time, which leads to the formation of large amounts of hydrated minerals in the case of lowering the temperature, and, conversely, in the case of increasing the temperature in reversible dehydration for a number of minerals, as shown by us in a number of experiments. It is known that structurally and chemically complex hydroxysalt minerals with various metals, as a rule, are formed as a result of secondary geological processes, such as oxidation zones, crystallisation from aqueous solutions, etc., i.e. the presence of water in the systems is responsible for the occurrence of complex structural architectures. These complex minerals almost invariably contain water or hydroxyl groups. In respect to complexity, fumarolic anhydrous copper minerals with sulfate anions, and especially those containing additional oxygen atoms, form a separate group of primary minerals that reflect both the general complexity of the structures and the complexity of the transformation processes. Moreover, some of the structurally complex anhydrous copper sulfates (euchlorine, alumoklyuchevskite and saranchinaite) can be considered not as rare fumarolic accessory minerals, but rather as rock-forming in primary exhalative mineral assemblages. It is worth noting that H_2O is the main component of gases and an agent for the transport of transition metals in post-eruptive processes on the scoria cones of the Tolbachik volcano (Fedotov and Markhinin, 1983). Above some temperature limit, water is supposed to act mostly as a chemical transporting agent; if the deposition temperature is relatively high, one can expect formation of anhydrous species. Below this limit, formation of hydrated species becomes possible. At temperatures close to ambient, it would be difficult, if ever possible, to discriminate the effects of exhaled ('intrinsic') and atmospheric ('extrinsic') water.

Acknowledgements. We are grateful to Ferdinando Bosi and two anonymous reviewers for valuable comments. This work was financially supported by the Russian Science Foundation through the grant 16-17-10085. Technical support by the SPbSU X-ray Diffraction and Geomodel Resource Centers is gratefully acknowledged. O.I.S. was supported by the internal SPbSU travel grant to the University of Kiel.

Supplementary material. To view supplementary material for this article, please visit https://doi.org/10.1180/mgm.2021.11

References

Altheide T., Chevrier V., Nicholson C. and Denson J. (2009) Experimental investigation of the stability and evaporation of sulfate and chloride brines on Mars. *Earth and Planetary Science Letters*, **282**, 69–78.

Bacon G.E. and Titterton D.H. (1975) Neutron-diffraction studies of $CuSO_4{\cdot}5(H_2O)$ and $CuSO_4{\cdot}5(D_2O)$. *Zeitschrift für Kristallographie*, **141**, 330–341.

Balassone G., Petti C., Mondillo N., Panikorovskii T.L., de Gennaro R., Cappelletti P., Altomare A., Corriero N., Cangiano M. and D'Orazio L. (2019) Copper minerals at Vesuvius volcano (Southern Italy): a mineralogical review. *Minerals*, **9**, 730.

Baur W.H. (1962) Zur Kristallchemie der Salzhydrate. Die Kristallstrukturen von $MgSO_4{\cdot}4(H_2O)$ (Leonhardtit) und $FeSO_4{\cdot}4(H_2O)$ (Rozenit). *Acta Crystallographica*, **15**, 815–826.

Baur W.H. and Rolin J.L. (1972) Salt hydrates. IX. The comparison of the crystal structure of magnesium sulfate pentahydrate with copper sulfate pentahydrate and magnesium chromate pentahydrate. *Acta Crystallographica*, **B28**, 1448–1455.

Bosi F., Belardi G. and Ballirano P. (2009) Structural features in Tutton's salts $K_2[M^{2+}(H_2O)_6](SO_4)_2$, with M^{2+}= Mg, Fe, Co, Ni, Cu, and Zn. *American Mineralogist*, **94**, 74–82.

Brese N.E., O'Keeffe M., Ramakrishna B.L. and Von Dreele R.B. (1990) Low-temperature structures of CuO and AgO and their relationships to those of MgO and PdO. *Journal of Solid State Chemistry*, **89**, 184–190.

Bruker. (2014) *TOPAS, Version 5.0*. Bruker AXS Inc, Madison, USA.

Calleri M., Gavetti A., Ivaldi G. and Rubbo M. (1984) Synthetic epsomite, $MgSO_4(H_2O)_7$: absolute configuration and surface features of the complementary {111} forms. *Acta Crystallographica*, **B40**, 218–222.

Cheng L., Li W., Li Y., Yang Y., Li Y., Cheng Y. and Song D. (2019) Thermal analysis and decomposition kinetics of the dehydration of copper sulfate pentahydrate. *Journal of Thermal Analysis and Calorimetry*, **135**, 2697–2703.

Chipera S.J. and Vaniman D.T. (2007) Experimental stability of magnesium sulfate hydrates that may be present on Mars. *Geochimica et Cosmochimica Acta*, **71**, 241–250.

Effenberger H. (1985) $Cu_2O(SO_4)$, Dolerophanite: refinement of the crystal structure with a comparison of $[OCu(II)_4]$ tetrahedra in inorganic compounds. *Monatshefte für Chemie*, **116**, 927–931.

Fan X.-F., Sun H.-D., Shen Z.-X., Kuo J.-L. and Lu Y.-M. (2008) A first-principle analysis on the phase stabilities, chemical bonds and band gaps of wurtzite structure $A_xZn_{1-x}O$ alloys (A = Ca, Cd, Mg). *Journal of Physics: Condensed Matter*, **20**, 235221.

Fedotov S.A. and Markhinin Y.K. (editors) (1983) *The Great Tolbachik Fissure Eruption*. Cambridge University Press, New York.

Fischer W. and Hellner E. (1964) Ueber die Struktur des Vanthoffits. *Acta Crystallographica*, **17**, 1613–1613.

Gorskaya M.G., Vergasova L.P., Filatov S.K., Rolich D.V. and Ananiev V.V. (1995) Alumoklyuchevskite, $K_3Cu_3AlO_2(SO_4)_4$, a new oxysulfate of K, Cu, and Al from volcanic exhalations, Kamchatka, Russia. *Zapiski Rossiiskogo Mineralogicheskogo Obshchestva*, **124**, 95–100.

Grevel K.-D. and Majzlan J. (2009) Internally consistent thermodynamic data for magnesium sulfate hydrates. *Geochimica et Cosmochimica Acta*, **73**, 6805–6815.

Hawthorne F.C. and Ferguson R.B. (1975) Refinement of the crystal structure of kröhnkite. *Acta Crystallographica*, **B31**, 1753–1755.

Hawthorne F.C., Groat L.A. and Eby R.K. (1989) Antlerite, $Cu_3SO_4(OH)_4$, a heteropolyhedral wallpaper structure. *The Canadian Mineralogist*, **27**, 205–209.

Hazen R.M., Papineau D., Bleeker W., Downs R.T., Ferry J.M., McCoy T.J., Sverjensky D.A. and Yang H. (2008) Mineral evolution. *American Mineralogist*, **93**, 1693–1720.

Hughes J.M. and Stoiber R.E. (1985) Vanadium sublimates from the fumaroles of Izalco Volcano, El Salvador. *Journal of Volcanology and Geothermal Research*, **24**, 283–291.

Kahler E. (1962) Die Kristallstruktur von Dolerophanit, $Cu_2O(SO_4)$, ein Beispiel fuer 5 Koordiniertes Kupfer. *Naturwissenschaften*, **49**, 298.

Krivovichev S.V. (2013) Structural complexity of minerals: information storage and processing in the mineral world. *Mineralogical Magazine*, **77**, 275–326.

Krivovichev S.V. (2014) Which inorganic structures are the most complex? *Angewandte Chemie – International Edition*, **53**, 654–661.

Krivovichev S.V., Mentré O., Siidra O.I., Colmont M. and Filatov S.K. (2013) Anion-centered tetrahedra in inorganic compounds. *Chemical Reviews*, **113**, 6459–6535.

Lander L., Rousse G., Batuk D., Colin C.V., Dalla Corte D.A. and Tarascon J.-M. (2017) Synthesis, structure, and electrochemical properties of K-based sulfates $K_2M_2(SO_4)_3$ with M = Fe and Cu. *Inorganic Chemistry*, **56**, 2013–2021.

Lindström N., Talreja T., Linnow K., Stahlbuhk A. and Steiger M. (2016) Crystallization behavior of Na_2SO_4 – $MgSO_4$ salt mixtures in sandstone and comparison to single salt behavior. *Applied Geochemistry*, **69**, 50–70.

Ma H., Bish D.L., Wang H.W. and Chipera S.J. (2009) Determination of the crystal structure of sanderite, $MgSO_4{\cdot}2H_2O$, by X-ray powder diffraction and the charge flipping method. *American Mineralogist*, **94**, 622–625.

Menyailov I.A. and Nikitina L.P. (1980a) Chemistry and metal contents of magmatic gases: the New Tolbachik Volcanoes case (Kamchatka). *Bulletin of Volcanology*, **43**, 195–205.

Menyailov I.A., Nikitina L.P. and Shapar V.N. (1980b) *Geochemical features of exhalations of Great Tolbachik Fissure Eruption*. Nauka, Moscow [in Russian].

Mills S.J., Wilson S.A., Dipple G.M. and Raudsepp M. (2010) The decomposition of konyaite: Importance in CO_2 in mine tailings. *Mineralogical Magazine*, **74**, 903–917.

Mitev P.D., Gajewski G. and Hermansson K. (2009) Anharmonic OH vibrations in brucite: small pressure-induced redshift in the range 0–22 GPa. *American Mineralogist*, **94**, 1687–1697.

Nagase K., Yokobayashi H. and Sone K. (1978) Spectrophotometric and thermoanalytical studies on the dehydration of copper (ii) sulfate and its double salts. *Thermochimica Acta*, **23**, 283–291.

Nazarchuk E.V., Siidra O.I., Agakhanov A.A., Lukina E.A., Avdontseva E.Yu. and Karpov G.A. (2018) Itelmenite, $Na_2CuMg_2(SO_4)_4$, a New anhydrous sulfate mineral from the Tolbachik Volcano. *Mineralogical Magazine*, **82**, 1233–1241.

Nazarchuk E.V., Siidra O.I., Nekrasova D.O., Shilovskikh V.V., Borisov A.S. and Avdontseva E.Yu. (2020) Glikinite, $Zn_3O(SO_4)_2$, a new anhydrous zinc oxysulfate mineral structurally based on OZn_4 tetrahedra. *Mineralogical Magazine*, **84**, 563–567.

Nordstrom D.K. (1982) The effect of sulfate on aluminum concentrations in natural waters: some stability relations in the system Al_2O_3 – H_2O – SO_3 at 298 K. *Geochimica et Cosmochimica Acta*, **46**, 618–692.

Pautov L.A., Mirakov M.A., Siidra O.I., Faiziev A.R., Nazarchuk E.V., Karpenko V.Yu. and Makhmadsharif S. (2020) Falgarite, $K_4(VO)_3(SO_4)_5$, a new mineral from sublimates of a natural underground coal fire at the tract of Kukhi-Malik, Fan-Yagnob Coal Deposit, Tajikistan. *Mineralogical Magazine*, **84**, 455–462.

Pekov I.V., Koshlyakova N.N., Zubkova N.V., Lykova I.S., Britvin S.N., Yapaskurt V.O., Agakhanov A.A., Shchipalkina N.V., Turchkova A.G. and Sidorov E.G. (2018a) Fumarolic arsenates – a special type of arsenic mineralization. *European Journal of Mineralogy*, **30**, 305–322.

Pekov I.V., Zubkova N.V. and Pushcharovsky D.Y. (2018b) Copper minerals from volcanic exhalations – a unique family of natural compounds: crystal-chemical review. *Acta Crystallographica*, **B74**, 502–518.

Pekov I.V., Zubkova N.V., Yapaskurt V.O., Belakovskiy D.I., Chukanov N.V., Kasatkin A.V., Kuznetsov A.M. and Pushcharovsky D.Y. (2013) Kobyashevite, $Cu_5(SO_4)_2(OH)_6{\cdot}4H_2O$, a new devilline-group mineral from the Vishnevye Mountains, South Urals, Russia. *Mineralogy and Petrology*, **107**, 201–210.

Ramamurthy P. and Secco E.A. (1970) Studies on metal hydroxy compounds. XII. Thermal analyses, decomposition kinetics, and infrared spectra of copper basic oxysalts. *Canadian Journal of Chemistry*, **48**, 3510–3519.

Rasmussen S.E., Jorgensen J.E. and Lundtoft B. (1996) Structures and phase transitions of Na_2SO_4. *Journal of Applied Crystallography*, **29**, 42–47.

Rentzeperis P.J. and Soldatos C.T. (1958) The crystal structure of the anhydrous magnesium sulphate. *Acta Crystallographica*, **11**, 686–688.

Siidra O.I., Vergasova L.P., Kretser Y.L., Polekhovsky Y.S., Filatov S.K. and Krivovichev S.V. (2014b) Unique thallium mineralization in the fumaroles of Tolbachik Volcano, Kamchatka peninsula, Russia. II. Karpovite, $Tl_2VO(SO_4)_2(H_2O)$. *Mineralogical Magazine*, **78**, 1699–1709.

Siidra O.I., Vergasova L.P., Kretser Y.L., Polekhovsky Y.S., Filatov S.K. and Krivovichev S.V. (2014c) Unique thallium mineralization in the fumaroles of Tolbachik Volcano, Kamchatka peninsula, Russia. III. Evdokimovite, $Tl_4(VO)_3(SO_4)_5(H_2O)_5$. *Mineralogical Magazine*, **78**, 1711–1724.

Siidra O.I., Vergasova L.P., Krivovichev S.V., Kretser Y.L., Zaitsev A.N. and Filatov S.K. (2014a) Unique thallium mineralization in the fumaroles of Tolbachik Volcano, Kamchatka peninsula, Russia. I. Markhininite, $TlBi(SO_4)_2$. *Mineralogical Magazine*, **78**, 1687–1698.

Siidra O.I., Borisov A.S., Lukina E.A., Depmeier W., Platonova N.V., Colmont M. and Nekrasova D.O. (2019a) Reversible hydration/dehydration and thermal expansion of euchlorine, ideally $KNaCu_3O(SO_4)_3$. *Physics and Chemistry of Minerals*, **46**, 403–416.

Siidra O.I., Lukina E.A., Nazarchuk E.V., Depmeier W., Bubnova R.S., Agakhanov A.A., Avdontseva E.Yu., Filatov S.K. and Kovrugin V.M.

https://doi.org/10.1180/mgm.2021.11 Published online by Cambridge University Press

(2018a) Saranchinaite, $Na_2Cu(SO_4)_2$, a new exhalative mineral from Tolbachik Volcano, Kamchatka, Russia, and a product of the reversible dehydration of kröhnkite, $Na_2Cu(SO_4)_2(H_2O)_2$. *Mineralogical Magazine*, **82**, 257–274.

Siidra O.I., Nazarchuk E.V., Agakhanov A.A., Lukina E.A., Zaitsev A.N., Turner R., Filatov S.K., Pekov I.V., Karpov G.A. and Yapaskurt V.O. (2018b) Hermannjahnite, $CuZn(SO_4)_2$, a new mineral with chalcocyanite derivative structure from the Naboko Scoria Cone of the 2012–2013 Fissure Eruption at Tolbachik Volcano, Kamchatka, Russia. *Mineralogy and Petrology*, **112**, 123–134.

Siidra O.I., Nazarchuk E.V., Lukina E.A., Zaitsev A.N. and Shilovskikh V.V. (2018c) Belousovite, $KZn(SO_4)Cl$, a new sulfate mineral from the Tolbachik Volcano with apophyllite sheet-topology. *Mineralogical Magazine*, **82**, 1079–1088.

Siidra O.I., Nazarchuk E.V., Zaitsev A.N. and Shilovskikh V.V. (2020a) Majzlanite, $K_2Na(ZnNa)Ca(SO_4)_4$, a new anhydrous sulfate mineral with complex cation substitutions from Tolbachik Volcano. *Mineralogical Magazine*, **84**, 153–158.

Siidra O.I., Nazarchuk E.V., Zaitsev A.N. and Vlasenko N.S. (2020b) Koryakite, $NaKMg_2Al_2(SO_4)_6$, a new NASICON-related anhydrous sulfate mineral from Tolbachik Volcano. *Mineralogical Magazine*, **84**, 283–287.

Siidra O.I., Nazarchuk E.V., Zaitsev A.N., Lukina E.A., Avdontseva E.Yu., Vergasova L.P., Vlasenko N.S., Filatov S.K., Turner R. and Karpov G.A. (2017) Copper oxosulphates from fumaroles of Tolbachik Volcano: Puninite, $Na_2Cu_3O(SO_4)_3$ – a new mineral species and structure refinements of kamchatkite and alumoklyuchevskite. *European Journal of Mineralogy*, **29**, 499–510.

Siidra O.I., Nazarchuk E.V., Agakhanov A.A. and Polekhovsky Yu.S. (2019c) Aleutite $[Cu_5O_2](AsO_4)(VO_4)\cdot(Cu_{0.5}\square_{0.5})Cl$, a new complex salt-inclusion mineral with Cu^{2+} substructure derived from Kagome-net. *Mineralogical Magazine*, **83**, 847–853.

Siidra O.I., Nazarchuk E.V., Zaitsev A.N., Polekhovsky Yu.S., Wenzel T. and Spratt J. (2019b) Dokuchaevite, $Cu_8O_2(VO_4)_3Cl_3$, a new mineral with remarkably diverse Cu^{2+} mixed-ligand coordination environments. *Mineralogical Magazine*, **83**, 749–755.

Sklute E.C., Rogers A.D., Gregerson J.C., Jensen H.B., Reeder R.J. and Dyar M.D. (2018) Amorphous salts formed from rapid dehydration of multicomponent chloride and ferric sulfate brines: implications for Mars. *Icarus*, **302**, 285–295.

Stanimirova T. and Ivanova K. (2019) Transformation of ktenasite-type minerals to langite, posnjakite, and brochantite under water treatment. *Comptes rendus de l'Academie bulgare des Sciences*, **72**, 768–776.

Steiger M., Linnow K., Ehrhardt D. and Rohde M. (2011) Decomposition reactions of magnesium sulfate hydrates and phase equilibria in the $MgSO_4$–H_2O and Na^+–Mg^{2+}–Cl^-–SO_4^{2-}–H_2O systems with implication for Mars. *Geochimica et Cosmochimica Acta*, **75**, 3600–3626.

Tanaka H. and Koga N. (1988) Preparation and thermal decomposition of basic copper (II) sulfates. *Thermochimica Acta*, **133**, 221–226.

Ting V.P., Henry P.F., Schmidtmann M., Wilson C.C. and Weller M.T. (2009) In situ neutron powder diffraction and structure determination in controlled humidities. *Chemical Communications*, **48**, 7527–7529.

Uzunov I., Klissurski D. and Teocharov L. (1995) Thermal decomposition of basic copper sulfate monohydrate. *Journal of Thermal Analysis*, **44**, 685–696.

Vaniman D.T., Bish D.L., Chipera S.J., Fialips C.I., Carey J.W. and Feldman W.G. (2004) Magnesium sulphate salts and the history of Water on Mars. *Nature*, **431**, 663–665.

Vergasova L.P. and Filatov S.K. (2012) New mineral species in products of fumarole activity of the Great Tolbachik Fissure Eruption. *Journal of Volcanology and Seismology*, **6**, 281–289.

Vergasova L.P. and Filatov S.K. (2016) A study of volcanogenic exhalation mineralization. *Journal of Volcanology and Seismology*, **10**, 71–85.

Wildner M. (1992) On the geometry of $Co(II)O_6$ polyhedra in inorganic compounds. *Zeitschrift für Kristallographie*, **202**, 51–70.

Xu W., Tosca N.J., Mclennan S.M. and Parise J.B. (2009) Humidity-induced phase transitions of ferric sulfate minerals studied by in situ and ex situ X-ray diffraction. *American Mineralogist*, **94**, 1629–1637.

Yoder C.H., Agee T.M., Ginion K.E., Hofmann A.E., Ewanichak J.E., Schaeffer C.D. Jr., Carroll M.J., Schaeffer R.W. and McCaffrey P.F. (2007) The relative stabilities of the copper hydroxyl sulfates. *Mineralogical Magazine*, **71**, 571–577.

Zahrobsky R.F. and Baur W.H. (1968) On the crystal chemistry of salt hydrates. V. The determination of the crystal structure of $CuSO_4\cdot3H_2O$ (bonattite). *Acta Crystallographica*, **B24**, 508–513.

Zalkin A., Ruben H. and Templeton D.H. (1964) The crystal structure and hydrogen bonding of magnesium sulfate hexahydrate. *Acta Crystallographica*, **17**, 235–240.

Zhou H.A., Liu Z., Ang S.S. and Zhang J.-J. (2020) Synthesis, structure, and electrochemical performances of a novel three-dimensional framework $K_2[Cu(SO_4)_2]$. *Solid State Sciences*, **100**, 106104.

https://doi.org/10.1180/mgm.2021.11 Published online by Cambridge University Press